ACADEMIC PRESS

Available online at www.sciencedirect.com

SCIENCE DIRECT®

Journal of Sound and Vibration 266 (2003) 75–92

JOURNAL OF SOUND AND VIBRATION

www.elsevier.com/locate/jsvi

Computing the sound power in non-uniform flow

O.V. Atassi

Pratt & Whitney, 400 Main Street Engineering Building, M/S 163-29, East Hartford, CT 06108, USA

Received 14 January 2002; accepted 2 September 2002

Abstract

An expression for the sound power in an annular duct with swirling mean flow is derived in the high-frequency limit relevant to fan aeroacoustics. The sound power is expressed in terms of the duct normal modes which are computed for several mean flows. It is shown that the mean flow non-uniformity modifies both the pressure-dominated modes and the expression for the sound power. The pressure-dominated modes are not orthogonal and thus one must account for interference between the different radial modes. The interference effects are small for the case of a potential mean flow. For a vortical mean flow interference terms may become significant.

1. Introduction

The mean flow velocity of fan engines is characterized by significant swirl and radial variations in both the axial and swirl components. The work done by the fan blades may also produce radial variations in the total enthalpy. Representative results from a Reynolds-averaged Navier–Stokes calculation for the circumferentially averaged flow downstream of a fan are shown in Fig. 1. The large variations in the tip region are associated with the tip vortex shed from the fan.

Current fan noise schemes compute the wave modes and sound power in a constant area annular duct by assuming the mean flow is axial and uniform [1] or that the annulus is narrow [2,3]. The normal mode analysis can then be used to determine stator vane counts for optimal noise control such as cutting off blade passing frequency tone noise [4].

In order to incorporate non-uniform mean flow effects, a normal mode analysis of such flows must be carried out. Recent studies, to account for swirl, have assumed simple analytic models for the mean flow swirl which consist of combinations of free vortex and rigid body swirl [5–7]. These treatments assume uniform total enthalpy and entropy. The results show that the centrifugal and Coriolis effects create force imbalances which couple the acoustic, vortical and entropic flow

E-mail address: atassio@pweh.com (O.V. Atassi).

0022-460X/03/$ - see front matter
doi:10.1016/S0022-460X(02)01448-7

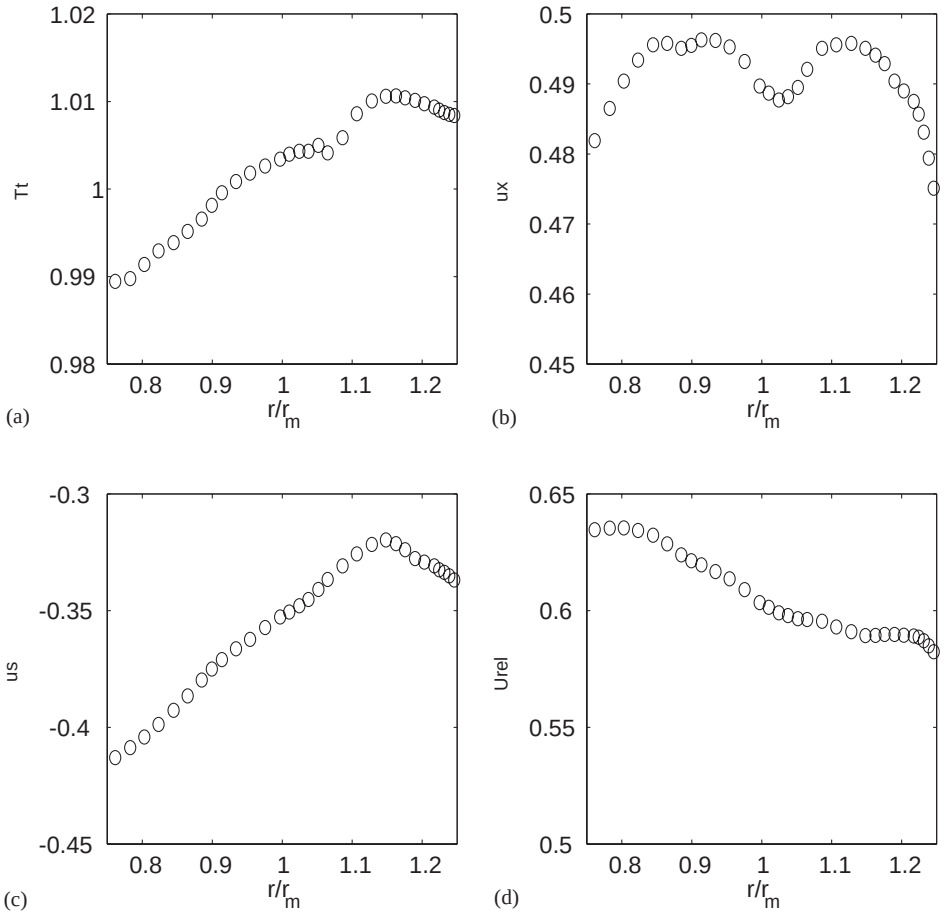

Fig. 1. The radial profile of the mean flow in a plane lying between a fan and an exit guide vane. The computational results were obtained using a Reynolds averaged Navier–Stokes code and show the strongest radial variations in the tip region of the annulus where the tip vortex of the fan lies. The total enthalpy is shown in (a) and the axial, swirl and relative velocity are shown in (b), (c) and (d), respectively.

disturbances. However, for the high frequencies relevant to fan tone noise, the coupling is weak [6,8], i.e., the acoustic modes have small vorticity content and the vortical modes have small pressure content. Recently [9], the eigenanalysis has been generalized to flows with non-uniform enthalpy enabling the study of the effects of non-uniform blade loading distributions on the propagation of sound.

Often one wishes to determine via experiment or computation the spectral composition and the time-averaged intensity flux of sound propagating in a duct [10]. The utility of computing the flux of sound intensity is that, under certain conditions, it is a conserved quantity and so different measurements of the sound power which are taken at different axial locations can be compared. Conservation of energy can also be used to understand the process by which acoustic energy is transferred between a sound wave and the mean field [11] or the effect of convection of an acoustic source on sound radiation [12]. In order to determine the intensity of sound, we must separate

from the total unsteady field the acoustic field and determine the energy flux of the acoustic waves. In this paper, we derive an energy relation for acoustic waves propagating in a non-uniform mean flow and we use the normal mode solutions to compute the sound power.

For small-amplitude disturbances to an isentropic irrotational flow an acoustic energy conservation equation can be derived from the Euler equations which depends only on first order quantities [13,14]. The intensity flux which results is conserved. Myers [15,16] derived the acoustic energy relation directly from the general energy equation and showed that the acoustic energy represents, to leading order, the energy carried by the unsteady disturbances. In the general case of a non-uniform mean flow, the time-averaged intensity flux is not conserved.

In order to study non-uniform mean flow effects on the propagation of sound energy, we start, in Section 3, from the acoustic energy equation for small-amplitude disturbances and derive a simplified relation valid in the high-frequency limit relevant to fan aeroacoustics. We note that the non-uniform mean flow, in addition to changing the aerodynamic interaction mechanism and the acoustic modes, also affects the expression for the acoustic energy. Moreover, as a result of the non-uniformity of the mean flow the duct radial modes are not orthogonal and therefore interference between the different radial modes will modify the computed sound intensity. In Section 4, we compute the acoustic power for a variety of isentropic mean flows and examine the effect of the mean flow swirl and vorticity on the propagation of acoustic energy in a duct.

2. Mathematical formulation

For a non-viscous, non-heat-conducting perfect gas with constant specific heats, the governing equations are the Euler equations. The flow variables are decomposed into a sum between their steady mean values and their unsteady perturbations,

$$\vec{U}(\mathbf{x},t)=\vec{U}_0(\mathbf{x})+\vec{u}(\vec{x},t),\quad p(\vec{x},t)=p_0(\vec{x})+p'(\vec{x},t),$$

$$\rho(\vec{x},t)=\rho_0(\vec{x})+\rho'(\vec{x},t), \tag{1}$$

where $\vec{x}$ represents any co-ordinate system, t represents time, $\vec{U}_0$, p_0, and ρ_0 are the steady mean velocity, pressure, density, and $\vec{u}$, p' and ρ' are the corresponding unsteady perturbation quantities. The unsteady quantities are assumed to be small such that $\{|\vec{u}(\vec{x},t)|,|p'|,|\rho'|\}\ll\{\vec{U}_0(\vec{x}),p_0,\rho_0\}$. We non-dimensionalize with respect to the mean radius of the duct, r_m, the mean density, ρ_m, and speed of sound, c_m, at the mean radius.

Substituting into the Euler equations, the equations governing the unsteady variables reduce to the following non-dimensional coupled system of linear equations [17]:

$$\frac{D_0}{Dt}\rho'+(\vec{u}\cdot\nabla)\rho_0+\rho_0\nabla\cdot\vec{u}+\rho'\nabla\cdot\vec{U}_0=0, \tag{2}$$

$$\rho_0\left(\frac{D_0}{Dt}\vec{u}+\vec{u}\cdot\nabla\vec{U}_0\right)+\rho'(\vec{U}_0\cdot\nabla\vec{U}_0)=-\nabla p', \tag{3}$$

$$\frac{D_0}{Dt}p'+\vec{u}\cdot\nabla p_0+\gamma p_0\nabla\cdot\vec{u}+\gamma p'\nabla\cdot\vec{U}_0=0, \tag{4}$$

where D_0/Dt is the mean flow material derivative

$$\frac{D_0}{Dt} \equiv \frac{\partial}{\partial t} + \vec{U}_0 \cdot \nabla. \tag{5}$$

Note the pressure, density and entropy are related by the equation of state and, as a result, the energy equation can also be expressed in terms of the entropy as

$$\frac{D_0}{Dt} s' + \vec{u} \cdot \nabla \vec{S}_0 = 0. \tag{6}$$

The impermeability condition is imposed at the hub and tip radii,

$$u_r = 0. \tag{7}$$

The mean flow is assumed axisymmetric and, away from the upstream and downstream blade rows where the geometry is modelled by a constant area annular duct, the axial mean flow gradients are assumed to be much smaller than the radial gradients. The azimuthal variations in the flow are then accounted for in the unsteady perturbation quantities. In such a flow region, mass conservation implies that the radial velocity is small and the non-dimensional mean flow velocity can be expressed in the form

$$\vec{U}_0(\vec{x}) = M_x(r)\mathbf{e}_x + M_s(r)\mathbf{e}_\theta, \tag{8}$$

where $\mathbf{e}_x$ and $\mathbf{e}_\theta$ represent unit vectors in the axial and circumferential directions, respectively, and $M_x(r) = U_x/c_m$ and $M_s(r) = U_s/c_m$. The mean flow is, in general, vortical with the vorticity given by

$$\vec{\zeta}_0 = \nabla \times \vec{U}_0 = \frac{1}{r}\frac{\mathrm{d}(rM_s)}{\mathrm{d}r}\mathbf{e}_x - \frac{\mathrm{d}M_x}{\mathrm{d}r}\mathbf{e}_\theta. \tag{9}$$

The stagnation enthalpy, velocity, vorticity, temperature and entropy are related by Crocco's equation,

$$\nabla H = \vec{U}_0 \times \vec{\zeta}_0 + T_0 \nabla S_0, \tag{10}$$

where H is the stagnation enthalpy, T_0 is the static temperature and S_0 is the entropy.

2.1. Normal mode expansion

Solutions to the linearized Euler equations are obtained in terms of eigenmodes. The normal mode analysis presented here follows Ref. [9] and is briefly reviewed here. The following Fourier expansion is assumed:

$$\{\rho', u_x, u_r, u_\theta, p'\}(x, r, \theta; t) = \int_{-\infty}^{\infty} \sum_{m=-\infty}^{\infty} \sum_{n=1}^{\infty} \{\rho_{mn}, X_{mn}(r), T_{mn}(r), R_{mn}(r), p_{mn}(r)\} \times e^{i(-\omega t + m\theta + k_{mn}x)}\, \mathrm{d}\omega, \tag{11}$$

where m, and n are integer modal numbers characterizing the circumferential and radial eigenmodes, respectively. Note that we solve for five variables and the perturbation entropy can be determined from the pressure and density using the equation of state. Since the equations are linear, each Fourier component can be considered separately. Substituting Eq. (11) into

Eqs. (2)–(4) gives the coupled system of equations governing the normal modes:

$$\Lambda_{mn}\rho_{mn} - \frac{1}{r}\frac{\mathrm{d}}{\mathrm{d}r}[(\rho_0 r)(\mathrm{i}R_{mn})] + \rho_0\left(\frac{m}{r}T_{mn} + k_{mn}X_{mn}\right) = 0, \tag{12}$$

$$\rho_0\left(\Lambda_{mn}X_{mn} - \frac{\mathrm{d}M_x}{\mathrm{d}r}\mathrm{i}R_{mn}\right) + k_{mn}p_{mn} = 0, \tag{13}$$

$$\rho_0\left(\Lambda_{mn}T_{mn} - \frac{1}{r}\frac{\mathrm{d}}{\mathrm{d}r}(rM_s)\mathrm{i}R_{mn}\right) + \frac{m}{r}p_{mn} = 0, \tag{14}$$

$$\rho_0\left(\Lambda_{mn}\mathrm{i}R_{mn} - \frac{2M_s}{r}T_{mn}\right) + \frac{\mathrm{d}p_{mn}}{\mathrm{d}r} - \frac{M_s^2}{r}p_{mn} = 0, \tag{15}$$

$$\Lambda_{mn}p_{mn} - \left(\frac{\mathrm{d}p_0}{\mathrm{d}r} + \frac{\gamma p_0}{r}\right)(\mathrm{i}R_{mn}) + \gamma p_0\left(\frac{m}{r}T_{mn} - \frac{\mathrm{d}R_{mn}}{\mathrm{d}r} + k_{mn}X_{mn}\right) = 0, \tag{16}$$

where the convective eigenvalue, Λ_{mn}, is defined by the expression

$$\Lambda_{mn} = -\omega + k_{mn}M_x + \frac{mM_s}{r}. \tag{17}$$

The boundary condition at the hub and tip radii is

$$R_{mn}(r) = 0. \tag{18}$$

The normal modes are normalized such that

$$\int_{r_h/r_m}^{r_t/r_m} r p_{mn} p_{mn}^{*}\,\mathrm{d}r = 1, \tag{19}$$

where $*$ denotes the complex conjugate. Note that unlike the uniform axial mean flow limit this is not a Sturm–Liouville eigenvalue problem. Therefore, there is no proof of completeness or orthogonality of the eigenfunctions. Moreover, the acoustic, vortical and entropic modes are coupled to each other through the mean flow gradients. Discretizing the normal mode equations leads to an algebraic system of equations of the form

$$[A]\mathbf{x} = k_{mn}[B]\mathbf{x}, \tag{20}$$

where $[A]$ and $[B]$ are real matrices resulting from Eqs. (12)–(15) and $\mathbf{x}$ is eigenvector representing the eigenfunctions $\rho_{mn}, X_{mn}, T_{mn}, \mathrm{i}R_{mn}$, and p_{mn}. Solutions to Eq. (20) are obtained using a combination of spectral and shooting methods which are described in Ref. [9].

3. Sound power in a non-uniform flow

The transport of energy by small-amplitude disturbances is governed by the conservation equation [16]

$$\frac{\partial E}{\partial t} + \nabla\cdot\vec{I} = G, \tag{21}$$

where the energy density, E, the energy flux vector, $\vec{I}$, and source term, G, are defined by

$$E \equiv \frac{p'\rho'}{2\rho_0} + (\rho_0|u|^2 + \rho'\vec{u}\cdot\vec{U}_0), \tag{22}$$

$$\vec{I} \equiv \left(\frac{p'}{\rho_0} + \vec{u}\cdot\vec{U}_0\right)(\rho_0\vec{u} + \rho'\vec{U}), \tag{23}$$

$$G \equiv \vec{u}\cdot[\vec{U}_0 \times (\rho_0\vec{\zeta}' - \vec{\zeta}_0\rho')] + \frac{(\vec{u} + \frac{\rho'}{\rho_0}\vec{U}_0)}{\rho_0}\cdot(\rho'\nabla p_0 - p'\nabla\rho_0) + \frac{1}{2\rho_0}\left(\rho'\frac{\partial p'}{\partial t} - p'\frac{\partial\rho'}{\partial t}\right).$$

From Eq. (8), the mean radial velocity is zero and the term, $\frac{\rho'}{\rho_0}\vec{U}_0\cdot(\rho'\nabla p_0 - p'\nabla\rho_0)$ vanishes. Note that the expressions for the energy and energy flux are second order expressions which depend only on first order quantities. As a result, the energy of the unsteady disturbances can be computed as a by-product of the linearized Euler equations. Expressing the last four terms in G in terms of the entropy, Eq. (21) becomes

$$\frac{\partial E}{\partial t} + \nabla\cdot\vec{I} = \vec{u}\cdot\left[\vec{U}_0 \times (\rho_0\vec{\zeta}' - \vec{\zeta}_0\rho') + \frac{1}{c_p}(p'\nabla S_0 - s'\nabla p_0)\right] + \frac{c_0^2}{2c_p}\left(\rho'\frac{\partial s'}{\partial t} - s'\frac{\partial\rho'}{\partial t}\right). \tag{24}$$

Eq. (24) shows that the disturbance field interacts with the mean flow and mean flow gradients to transfer energy between the mean flow and the propagating disturbances. Determining the terms on the right side of Eq. (24) is difficult because the unsteady perturbations are a small part of the total flow energy and there is no proof of completeness for a modal representation of the total unsteady flow.

3.1. Acoustic energy: high-frequency limit

In fan engine aeroacoustic calculations, the frequencies of the noise source are often high. For example, in tone noise the frequency is $nB\Omega$ where n is the harmonic index, B is the number of blades and Ω is the shaft rotation frequency. As a result, the characteristic acoustic wavelength is $\ell = c_m/(nB\Omega) = r_m/(nBM_m)$, where M_m is the rotational Mach number at the mean radius of the fan. However, variations in the mean flow are characterized by the mean radius of the duct. In the high-frequency limit, $\ell/r_m \ll 1$, the vorticity content of the acoustic waves is small [6]. To examine the relative order of the various terms in Eq. (24), we introduce the fast variables

$$\tilde{\vec{x}} = \vec{x}/\varepsilon, \tilde{t} = t/\varepsilon, \tag{25}$$

where $\varepsilon = \ell/r_m \ll 1$. Substituting the fast variables into the linearized energy equation we obtain

$$\frac{D_0}{D\tilde{t}}s' + \varepsilon(\vec{u}\cdot\tilde{\nabla})S_0 = 0, \tag{26}$$

where $D_0/D\tilde{t} \equiv \partial/\partial\tilde{t} + \vec{U}_0 \cdot \tilde{\nabla}$ and $\tilde{\nabla} = \varepsilon\nabla$. Eq. (26) shows that to leading order the unsteady entropy field is convected with the mean flow,

$$\frac{D_0}{D\tilde{t}} s' = 0, \tag{27}$$

over the small distance ℓ and that, if there is no source of entropy or entropy disturbances are not imposed upstream, the entropy disturbances generated by the mean entropy gradients in the flow will not contribute to the leading order unsteady field. Note that for isentropic flows Eq. (27) is exactly satisfied as is shown in Eq. (6).

Substituting Eq. (25) into Eq. (24), we obtain to leading order

$$\frac{\partial E}{\partial \tilde{t}} + \tilde{\nabla} \cdot \vec{I} = \vec{u} \cdot [\rho_0(\vec{U}_0 \times \vec{\tilde{\zeta}}')] + \frac{c_0^2}{2c_p}\left(\rho' \frac{\partial s'}{\partial \tilde{t}} - s' \frac{\partial \rho'}{\partial \tilde{t}}\right). \tag{28}$$

Note that $\vec{\tilde{\zeta}}' = \varepsilon\vec{\zeta}'$ is $O(|\vec{u}|)$. Eq. (28) shows that the acoustic intensity is no longer a conserved quantity as a consequence of the unsteady entropy and the interaction between the unsteady vorticity and the mean flow. For propagating acoustic waves, numerical results [6] suggest $\vec{\tilde{\zeta}}'$ is small and from Eq. (26) S' is $O(\varepsilon|\vec{u}|)$. As a result, the acoustic intensity is locally conserved over a distance, $O(\ell)$, which is small relative to the mean radius. In the general case, the disturbance field contains both acoustic and vortical parts. However, in the high-frequency limit, the two parts can be decoupled [6] since the pressure field associated with the nearly convected modes is small. Thus, taking only the acoustic part of the disturbance field and substituting into Eq. (28) we find that the acoustic energy is locally conserved, i.e.,

$$\left[\frac{\partial E}{\partial \tilde{t}} + \tilde{\nabla} \cdot \vec{I}\right]_A = 0, \tag{29}$$

where the subscript A denotes the acoustic part of the unsteady field.

3.1.1. The modal expression for the sound power

In this section, we express the sound power in terms of the propagating acoustic modes. Due to the non-orthogonality of the modes, interference terms exist in the sound power expression. When calculating the sound energy in an annular duct, we are interested in the mean flux of acoustic energy across an axial plane. The axial component of the intensity is expressed as

$$I_x = (p'/\rho_0 + M_x u_x + M_s u_\theta)(\rho_0 u_x + M_x p')sgn(n), \tag{30}$$

where $sgn(n) = 1$ for downstream propagating disturbances and $sgn(n) = -1$ for upstream propagating disturbances. Note the expression for the axial intensity has two terms which contain the swirl velocity. Substituting Eq. (11) into Eq. (30) and integrating across the axial surface we obtain the sound power in the duct,

$$\Pi = \pi\Re\left\{\sum_{n=1}^{n=N_r}\sum_{n'=1}^{n=N_r}\sum_{m=1}^{m=N_\theta} sgn(n) e^{i(k_{mn}-k_{mn'})x} \int_{r_h/r_m}^{r_t/r_m} r\left[\left(1+\frac{M_x^2}{c_0^2}\right)p_{mn}X_{mn'}^* + \frac{M_x}{\rho_0 c_0^2}p_{mn}p_{mn'}^* + \frac{M_x M_s}{c_0^2}p_{mn}T_{mn'}^* + \rho_0 M_x X_{mn}X_{mn'}^* + \rho_0 M_s X_{mn}T_{mn'}^*\right] dr\right\}, \tag{31}$$

where N_r and N_θ are the number of radial and circumferential propagating modes, $*$ is used to denote the complex conjugate and $\Re$ denotes the real part. Eq. (31) shows that for each circumferential mode, m, and radial mode, n, we sum the various contributions for each n'. Those radial modes for which $n' \neq n$ are referred to as interference terms and those modes for which $n' = n$ are non-interference terms.

When the mean flow is potential and isentropic, the time-averaged intensity flux is conserved. However, in a swirling mean flow, the eigenfunctions are not orthogonal. As a result, interference occurs between different radial modes. Note that the sound power varies with x for the interference modes $n \neq n'$. Thus, the conservation of sound power requires that the sum of the modal powers corresponding to the interference modes must be zero, i.e.,

$$\sum_{n=1}^{n=N_r} \sum_{n'=1}^{n=N_r} \int_{r_h/r_m}^{r_t/r_m} r\left[\left(1+\frac{M_x^2}{c_0^2}\right) p_{mn} X_{mn'}^* + \frac{M_x}{\rho_0 c_0^2} p_{mn} p_{mn'}^* + \frac{M_x M_s}{c_0^2} p_{mn} u_{mn'_\theta}^* + \rho_0 M_x X_{mn} X_{mn'}^* + \rho_0 M_s X_{mn} T_{mn'}^*\right] \mathrm{d}r = 0, \quad n \neq n'. \tag{32}$$

In the next section, we examine the extent to which Eq. (32) is satisfied for a variety of mean flow and determine which of the terms in Eq. (31) are the major contributors to the sound power.

4. Numerical results for swirling flow

We examine the effect of mean flow swirl on the modal sound power. For simplicity, we start by considering swirl distributions which consist of a linear combination of free vortex and rigid body swirl. In this case, the mean flow swirl distribution is characterized by a circulation, Γ, and a rigid body swirl defined by the angular velocity Ω. The swirl Mach number takes the form

$$M_s = M_\Omega + M_\Gamma, \tag{33}$$

where $M_\Omega = \Omega r/c_m$ and $M_\Gamma = \Gamma/(rc_m)$. If we further assume uniform enthalpy from hub to tip and isentropic flow, the axial component of velocity takes the form

$$M_x^2 = M_{xm}^2 - 2[\Omega^2(r^2-1) + 2\Omega\Gamma \ln(r)], \tag{34}$$

where M_{xm} is the axial Mach number at the mean radius of the duct. In the final subsection, we consider a mean flow profile with a non-uniform total enthalpy distribution.

In Section 4.1, we examine the case of free vortex swirl and in Section 4.2 we compute the modal power for a combination of free vortex and rigid body swirl to examine the degree to which coupling between vortical and acoustic disturbances modifies the conservation relation (29). In all cases, 100 points are used from hub to tip to compute the normal modes and the modal power. Finally in Section 4.3, a mean flow profile with non-uniform total enthalpy and swirl is studied.

4.1. A free vortex swirling flow

In a free vortex swirling flow, the acoustic disturbances propagating in a duct are purely potential and conserve acoustic energy exactly. We first examine this case and compute the contributions to the modal sound power from each of the terms in Eq. (31) to determine the major contributions to the sound power. The free vortex swirl distribution is shown in Fig. 2. In this

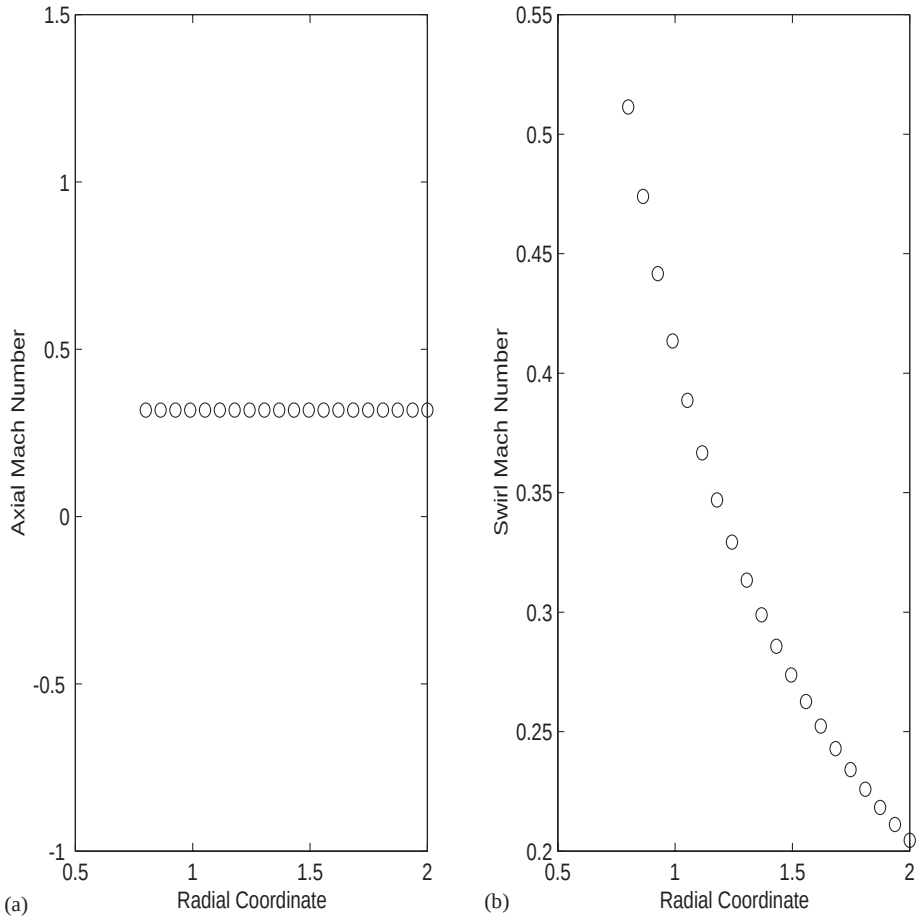

Fig. 2. Free vortex swirl distribution for a duct with hub–tip ratio of 0.4: (a) axial Mach number; (b) swirl Mach number.

case, the swirl velocity parameters are chosen so that $M_\Omega = 0$ and M_Γ at the hub is 0.52. The plot shows that the annulus extends from a non-dimensional radius of 0.8 to 2.0 and the swirl Mach number is inversely proportional to the radius. To conserve sound power, the sum of the contribution of each interference term in Eq. (32) must be zero so that there is no x-dependence in the sound power. Thus, although the eigenfunctions are not orthogonal, the summed contribution of the interference terms to the sound power should be negligible.

In Fig. 3, we show the contributions of each of the terms in the integral for the downstream propagating modes corresponding to a case with reduced frequency, $\omega = 20$ and spinning mode order, $m = -1$. For example, the contribution of the first term, $\int_{r_h/r_m}^{r_t/r_m} r(1 + \frac{M_x^2}{c_0^2}) p_{mn} X^*_{mn'} \, dr$, for a given ω, m and n is shown in each plot for each n'. The open circle, $+$ and $*$ correspond to the contributions of the first three terms in Eq. (32), respectively, and the x and diamond correspond to the fourth and fifth terms. The abscissa corresponds to the radial mode index n' and the ordinate represents the contribution of each term. The different figures correspond to different

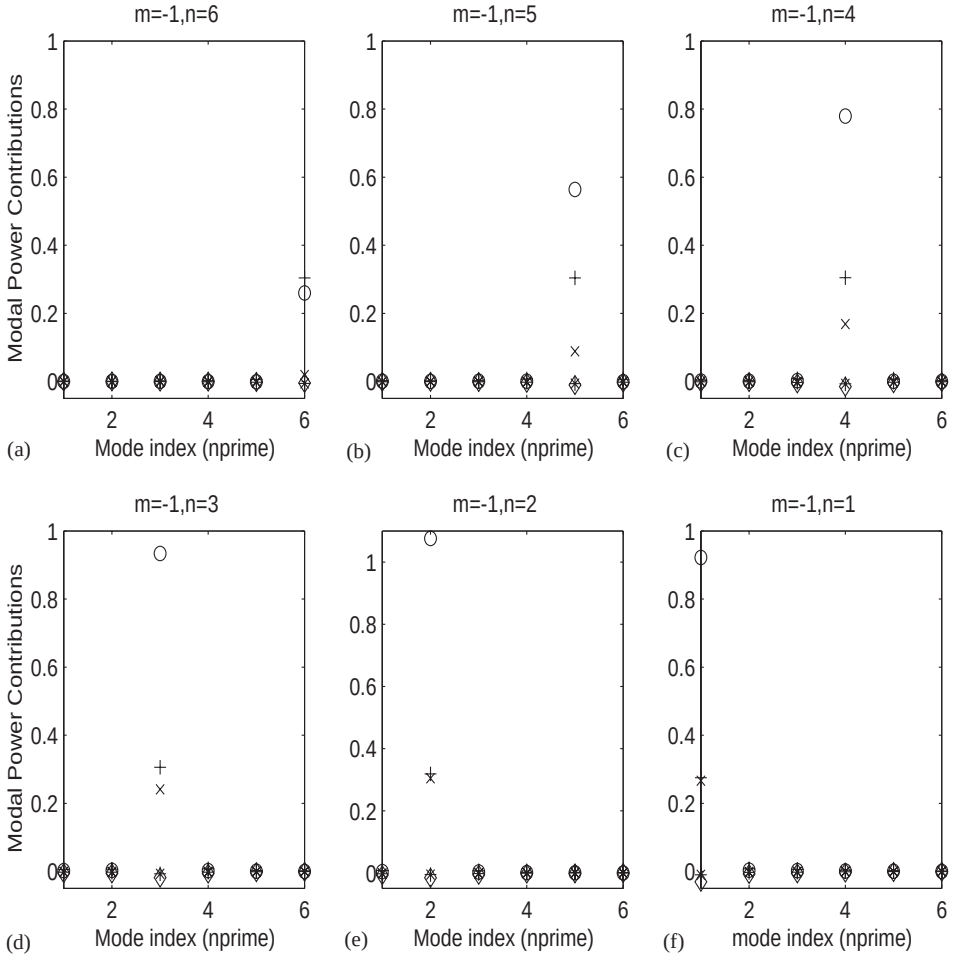

Fig. 3. Contributions of each term in Eq. (31) for the sound power of the downstream propagating duct modes. The reduced frequency is $\omega = 20$ and $m = -1$. The mean flow swirl is free vortex and the axial velocity is constant. The abscissa is the radial mode index, n', and each figure corresponds to the contribution of each radial mode n. The open circle, $+$, and $*$ correspond to the contributions of the first three terms in Eq. (31) and the x and diamond correspond to the fourth and fifth terms. (a)–(c) in the top row going from left to right correspond to $n = 6, 5, 4$ in descending order and (d)–(f) in the bottom row going from left to right correspond to $n = 3, 2, 1$.

radial mode orders, n, for a given spinning mode order, m. The index, n, describes the eigenfunction which has $n - 1$ zero crossings from the inner radius to the outer radius.

In this case, there exist six propagating modes. The contribution of the interference terms are quite small relative to the non-interference terms, $n = n'$. Also, the dominant contributions to the power result from the contributions of the first, second and fourth terms. For the highest order radial mode, $n = 6$, the first two terms contribute the most to modal power. As the mode order decreases, the contribution of the first term increases rapidly from a value of 0.25 to nearly one. The second term does not change appreciably for the various mode orders but the contribution of the fourth term becomes significant for the lower order radial modes. For this case, with low

spinning mode order, $m = -1$, the third and fifth terms which contain the swirl component of the mean velocity produce negligible contributions to the modal power. Summing the interference terms of the six modes we find the contribution is approximately 0.002 for each $n = 1, 2, \ldots, 6$ as opposed to the non-interference terms which result in a summed contribution of 7.3 to the power.

In Fig. 4, we consider a case with a reduced frequency of 30 and a larger spinning mode order, $m = -16$. In this case, there exist 10 propagating modes which are again ordered based on the number of zero crossings that occur between the hub and the tip. We show the first six upstream propagating modes which range from $n = 1$ to $n = 6$ in Fig. 4. Again the first, second and fourth terms contribute the most to the sound power. As in the previous case, the contribution of the

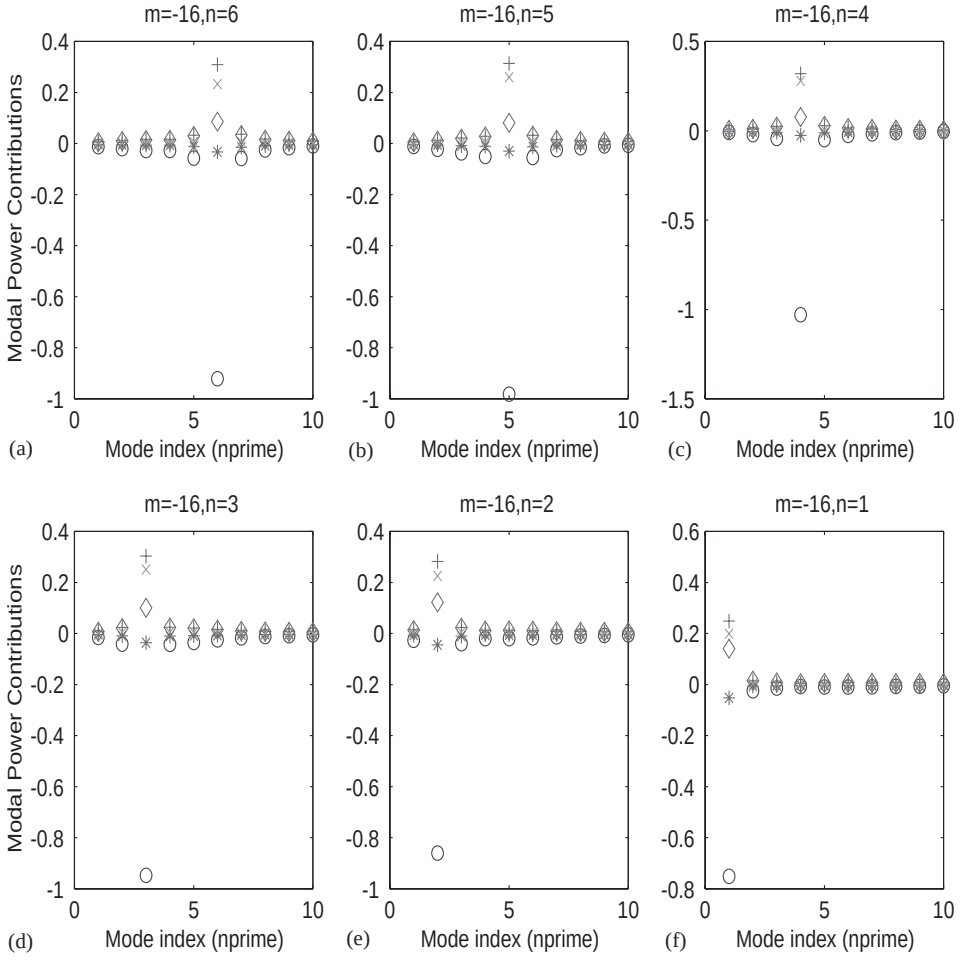

Fig. 4. Contributions of each term in Eq. (31) for the sound power of the upstream propagating duct modes. The mean flow swirl is free vortex and the axial velocity is constant. The reduced frequency is $\omega = 30$ and $m = -16$. The abscissa is the radial mode index, n' and each figure corresponds to the contribution of each radial mode n. The open circle, $+$, and $*$ correspond to the contributions of the first three terms in Eq. (31) and the x and diamond correspond to the fourth and fifth terms. (a)–(c) in the top row going from left to right correspond to $n = 6, 5, 4$ in descending order and (d)–(f) in the bottom row going from left to right correspond to $n = 3, 2, 1$.

fourth term increases slightly for the lower radial modes. Note that the contribution of the first term is negative because we are considering the upstream propagating modes and so the $sgn(n) = -1$ is yielding a positive sound power. Interference between the different radial modes is observed but the magnitude of the interference terms is small. The maximum contribution of the interference terms is 0.01. Interestingly, if we neglect the x-dependence and sum over all the modes $n \neq n'$, the summed contribution is zero to four significant digits. This is in contrast to the non-interference terms, $n = n'$, whose summed contribution is 2.77. The most significant interference contributions occurred from the modes adjacent to the $n = n'$ mode.

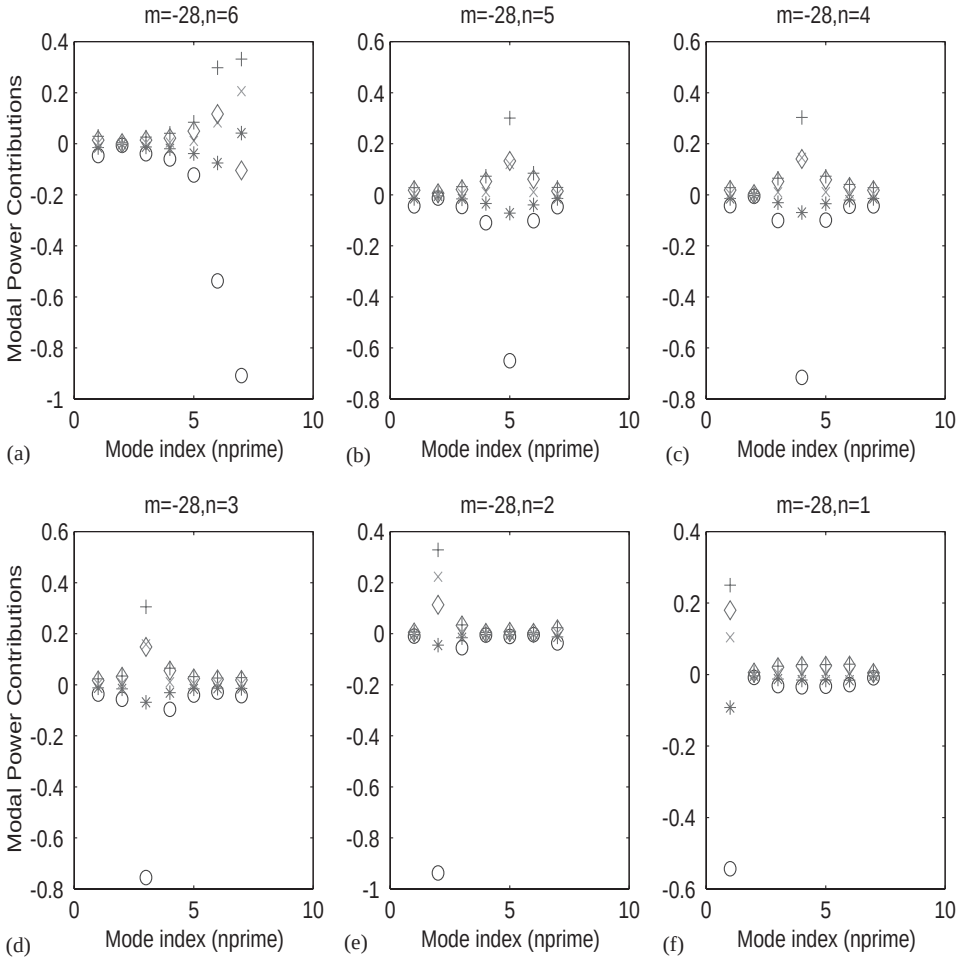

Fig. 5. Contributions of each term in Eq. (31) to the sound power of the upstream propagating duct modes. The mean flow swirl is free vortex and the axial velocity is constant. The reduced frequency is $\omega = 24.5$ and $m = -28$. The abscissa is the radial mode index, n' and each figure corresponds to the contribution of each radial mode n. The open circle, $+$, and $*$ correspond to the contributions of the first three terms in Eq. (31) and the x and diamond correspond to the fourth and fifth terms. (a)–(c) in the top row going from left to right correspond to $n = 6, 5, 4$ in descending order and (d)–(f) in the bottom row going from left to right correspond to $n = 3, 2, 1$.

We next consider a case with reduced frequency, 24.5 and spinning mode order $m = -28$ and look at the contributions to the sound power of the upstream propagating modes. In Fig. 5, we show the modal power contributions for each term in Eq. (31). In this case, the swirl Mach number plays a more significant role in the modal power. The third term in Eq. (31) is most significant for the higher order radial modes. Contributions from the interference terms are more evident in this case. However, when each of the terms in Eq. (31) is accounted for their maximum contributions remain small, i.e., 0.01. This is in contrast to the non-interference terms, $n = n'$, whose summed contribution is 1.77. If we neglect the x-dependence and sum over all the modes $n \neq n'$, the summed contribution is again zero to four significant digits.

In each of the three cases considered the numerical calculation of the sound power shows that it is nearly conserved. This is consistent with the potential mean flow used. In the next section, we consider a vortical mean flow where the sound power is not strictly conserved and examine, for high frequencies, the extent to which it is not conserved.

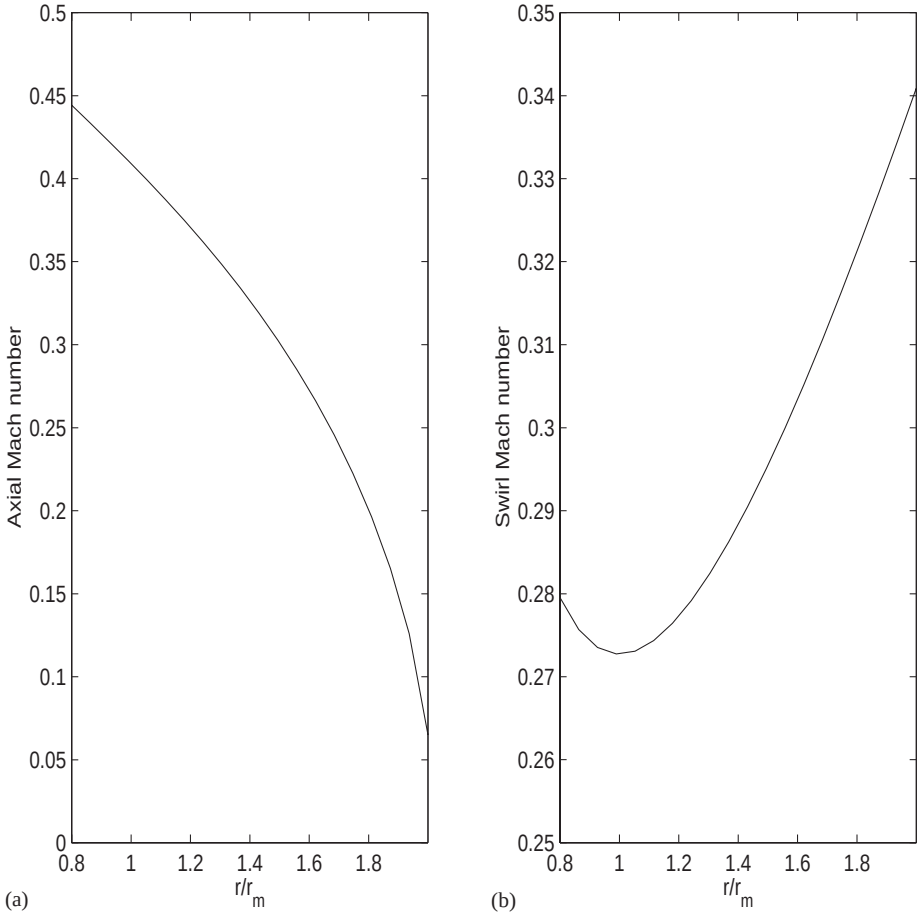

Fig. 6. Mean flow velocity distribution for a duct with hub–tip ratio of 0.4: (a) axial Mach number; (b) swirl Mach number.

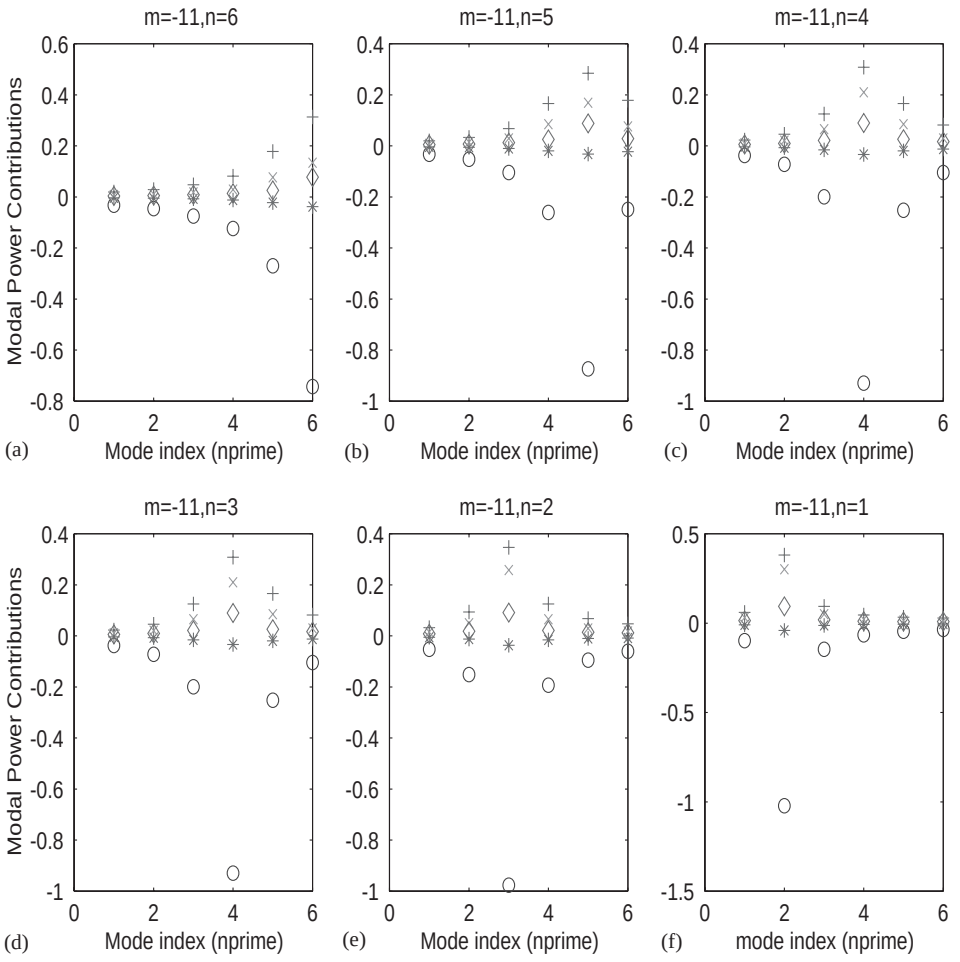

Fig. 7. Contributions of each term in Eq. (31) to the sound power of the upstream propagating duct modes. The mean flow is a combination of free vortex and rigid body swirl. The reduced frequency is $\omega = 20$ and $m = -11$. The abscissa is the radial mode index, n' and each figure corresponds to the contribution of each radial mode n. The open circle, $+$, and $*$ correspond to the contributions of the first three terms in Eq. (31) and the x and diamond correspond to the fourth and fifth terms. (a)–(c) in the top row going from left to right correspond to $n = 6, 5, 4$ in descending order and (d)–(f) in the bottom row going from left to right correspond to $n = 3, 2, 1$.

4.2. *Numerical results for a mean flow with streamwise vorticity*

We now consider a vortical mean flow that is a linear combination of rigid body and free vortex swirl. The mean flow velocity distribution is shown in Fig. 6. In this case, the swirl velocity parameters were chosen so that $M_\Omega = 0.11$ and $M_\Gamma = 0.17$ at the hub. As a result of the mean flow vorticity, the sound power is not strictly conserved and we expect interference effects to be more significant than the potential mean flow cases considered above. In Fig. 7, we show the contributions of each of the terms in the integral for the upstream propagating modes corresponding to a case with reduced frequency, $\omega = 20$ and spinning mode order, $m = -11$. Again, the open circle, $+$ and $*$ correspond to the contributions of the first three terms in Eq. (32),

respectively, and the x and diamond correspond to the fourth and fifth terms. The abscissa corresponds to the radial mode index n' and the ordinate represents the contribution of each term. The different figures correspond to different radial mode orders, n for a given spinning mode order, m. The index, n, describes the eigenfunction which has $n-1$ zero crossings from the hub to tip. In this case, there exist six propagating modes. As in the previous cases, the dominant contribution to the sound power comes from the first three terms in Eq. (32). The higher order modes ($n=6,5,4$) show significant contributions from the interference modes $n'=n\pm1$. The contributions of the other interference modes quickly decreases as $|n'-n|$ increases. Fig. 7 shows that the interference terms although large nearly cancel because the open circle in almost equal in magnitude but opposite in sign to the $+$ and x. As a result, the contributions of the interference

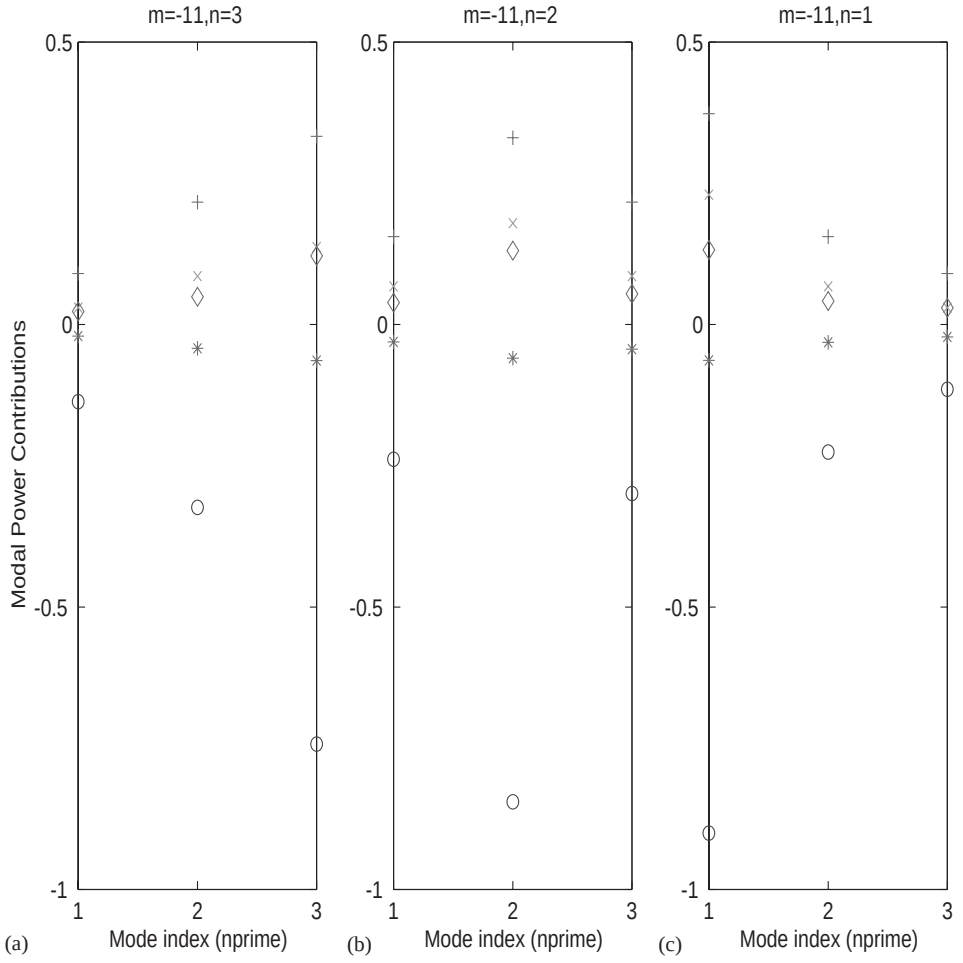

Fig. 8. Contributions of each term in Eq. (31) to the sound power of the upstream propagating duct modes. The mean flow is a combination of free vortex and rigid body swirl. The reduced frequency is $\omega=12$ and $m=-11$. The abscissa is the radial mode index, n', and each figure corresponds to the contribution of each radial mode n. The open circle, $+$, and $*$ correspond to the contributions of the first three terms in Eq. (31) and the x and diamond correspond to the fourth and fifth terms. (a)–(c) in the row going from left to right correspond to $n=3,2,1$ in descending order.

modes result in small modifications to the modal power of approximately 0.01 for each $n \neq n'$. The summed contribution of the non-interference modes is 1.816. Fig. 8 shows the contributions of each of the terms in the integral for the upstream propagating modes corresponding to a case with lower reduced frequency, $\omega = 12$, and spinning mode order, $m = -11$. Due to the lower frequency, there are only three propagating modes. Even for this frequency, the contributions of the interference modes largely cancel and result in modifications to the modal power of approximately 0.01 for $n = 1, 2, 3$, respectively. The summed contribution of the non-interference modes is 0.705.

4.3. Numerical results for a mean flow with non-uniform enthalpy

In this subsection, we compute the modal power in a mean flow where the mean flow vorticity does not lie completely in the streamwise direction. In this case, the total enthalpy varies from hub

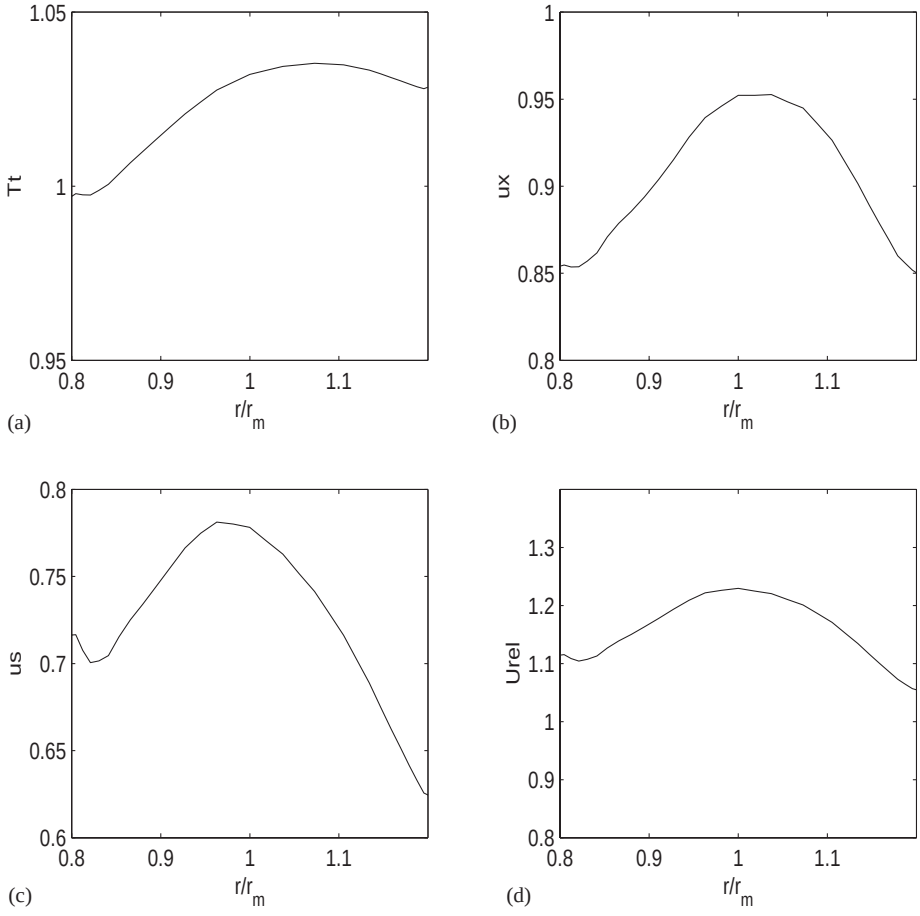

Fig. 9. The radial profile of the mean velocity and total enthalpy. The total enthalpy is shown in (a) and the axial, swirl and relative velocity are shown in (b), (c) and (d), respectively.

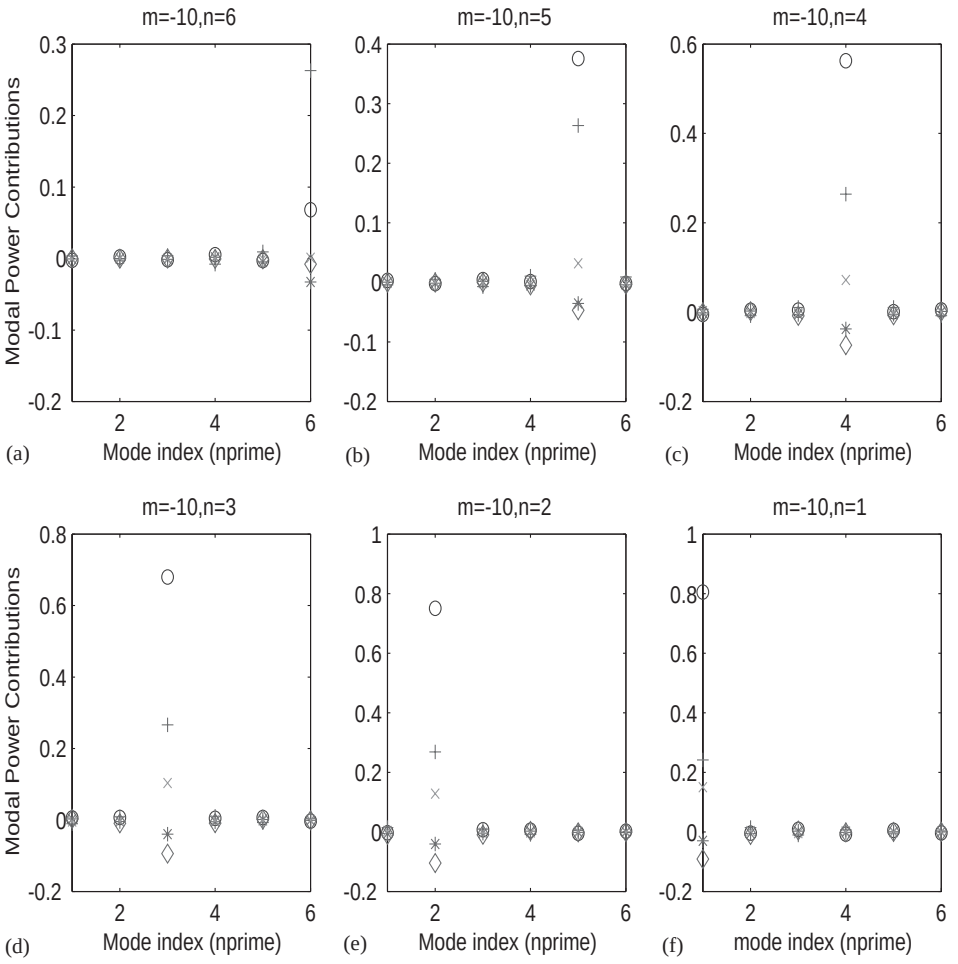

Fig. 10. Contributions of each term in Eq. (31) to the sound power of the upstream propagating duct modes. The reduced frequency is $\omega = 35$ and $m = -10$. The abscissa is the radial mode index, n', and each figure corresponds to the contribution of each radial mode n. (a)–(c) in the top row going from left to right correspond to $n = 6, 5, 4$ in descending order and (d)–(f) in the bottom row going from left to right correspond to $n = 3, 2, 1$.

to tip. The mean flow profiles for the velocity and total enthalpy are shown in Fig. 9. The swirl velocity increases with radius like the rigid body swirl case for $r/r_m < 1$ and decreases with radius for $r/r_m > 1$ like the free vortex swirl case. However, unlike those cases, the total temperature varies from hub to tip. Fig. 10 shows the contributions of each of the terms in the integral for the upstream propagating modes corresponding to a case with lower reduced frequency, $\omega = 35$, and spinning mode order, $m = -10$. At this reduced frequency, there are six propagating modes. The contributions of the interference modes are much smaller than the non-interference terms, again showing that the effect of the mean flow vorticity only slightly modifies the acoustic modal power.

5. Conclusions

An expression for the sound power was derived which is valid for non-uniform flows. For high-frequency disturbances, the propagation of sound energy is locally conserved. The dominant contributions to the sound power were computed for several mean flows. These results can be used to determine the major modal contributors to the sound power and determine the strength of the interaction between the mean flow and the acoustic waves. For the case of a free vortex mean flow swirl, interference effects were negligible. For the case of a vortical mean flow, interference effects are more significant but remain relatively small for large reduced frequencies in agreement with the high-frequency analysis presented in the paper. The conservation of the outgoing sound power can be used as a check on computational aeroacoustic schemes, which apply non-reflecting inlet/exit boundary conditions, to accurately propagate sound energy out of the computational domain.

Acknowledgements

This work was supported by NASA Glenn Research Center under AST 13 and monitored by Dennis Huff.

References

[1] M. Namba, Three-dimensional flow, in: Unsteady Turbomachinery Aerodynamics, AGARD-AG-298, 1987.
[2] D. Hanson, Theory for broadband noise of rotor and stator cascades with inhomogeneous inflow turbulence-including effects of lean and sweep, NASA CR-27727, 1999.
[3] S. Glegg, N. Walker, Fan noise from blades moving through boundary layer turbulence, in: Fifth AIAA/CEAS Aeroacoustics Conference, Seattle, USA, 1999.
[4] J.M. Tyler, T.G. Sofrin, Axial flow compressor noise studies, SAE Transactions 70 (1962) 309–332.
[5] V.V. Golubev, H.M. Atassi, Sound propagation in an annular duct with mean potential swirling flow, Journal of Sound and Vibration 198 (5) (1996) 601–616.
[6] V.V. Golubev, H.M. Atassi, Acoustic-vorticity waves in swirling flows, Journal of Sound and Vibration 209 (2) (1998) 203–222.
[7] K.A. Kousen, Eigenmode analysis of ducted flows with radially dependent axial and swirl components, in: First Joint CEAS/AIAA Aeroacoustics Conference, Munich, Germany, 1995, pp. 1085–1104.
[8] V.V. Golubev, H.M. Atassi, Unsteady swirling flows in annular cascades. Part I: evolution of incident disturbances, American Institute of Aeronautics and Astronautics Journal 38 (2000) 1142–1149.
[9] A.A. Ali, O.V. Atassi, H.M. Atassi, Acoustic eigenmodes in an annular duct with a general swirling flow, in: Sixth AIAA/CEAS Aeroacoustics Conference, Maui, Hawaii, 2000.
[10] U.W. Ganz, P.D. Joppa, T.J. Patten, D.F. Scharpf, Boeing 18 Fan Rig Broadband Noise Test, NASA CR 1998-208704.
[11] M.S. Howe, Conservation of energy in random media, with application to the theory of sound absorption by an inhomogeneous flexible plate, Proceedings of the Royal Society of London A 331 (1973) 479–496.
[12] M.S. Howe, Application of energy conservation to the solution of radiation problems involving uniformly convected source distributions, Journal of Sound & Vibration 43 (1975) 77–86.
[13] D.I. Blokhintsev, Acoustics of a nonhomogenuous moving medium, Translated NASA Technical Memorandum, No. 1399, 1956.
[14] C.L. Morfey, Acoustic energy in nonuniform flows, Journal of Sound & Vibration 14 (1971) 159–170.
[15] M.K. Myers, An exact energy corollary for homentropic flow, Journal of Sound & Vibration 109 (1986) 277–284.
[16] M.K. Myers, Transport of energy by disturbances in arbitrary steady flows, Journal of Fluid Mechanics 226 (1991) 383–400.
[17] M.E. Goldstein, Aeroacoustics, McGraw-Hill, 1976, p. 5.